Paper No.
C2020-15148

Removal of Iron Carbide in Turbulent Flow Conditions and Influence on Iron Carbonate Formation in Aqueous CO_2 Corrosion of Mild Steel

M. Di Bonaventura,[1] B. Brown, S. Nesic and M. Singer
Institute for Corrosion and Multiphase Technology
Department of Chemical and Biomolecular Engineering
Ohio University, Athens, OH 45701
USA

ABSTRACT

Iron carbide or cementite (Fe_3C) is often classified as a 'corrosion product' but it is originally found in the materials microstructure and, unlike iron carbonate ($FeCO_3$), it is not precipitated on the steel surface. Rather, it represents the leftover steel structure once the ferrite phase has been corroded away. Various researchers have found that Fe_3C acts as a diffusion barrier between iron and carbonate ions, which aids in the precipitation of $FeCO_3$. Previous studies have also considered various material compositions and microstructures favoring $FeCO_3$ formation. However, the effect of flow has not been considered previously although it plays a critical role in Fe_3C adherence to the steel surface as it is a fragile leftover layer. In this study, a ferritic-pearlitic UNS[2] G10180 material was exposed to flow velocities (0.4, 2 and 6m/s) and shear stresses (0.8, 20 and 100 Pa) in a thin rectangular flow channel at favorable layer formation conditions (T = 80°C, pH 6.6, $[Fe^{2+}]$ = 2 ppm, initial $S(FeCO_3) \approx 10$). A critical velocity for Fe_3C removal was identified, which further prevented the formation of $FeCO_3$, although it is fully expected that its value should depend on the operating conditions.

Key words: Iron carbide, Cementite, Shear stress, Iron carbonate, Carbon steel

[1] Current affiliation: BP America, 501 Westlake Park Blvd, Houston, TX 77079, USA
[2] Unified Numbering System for Metals and Alloys (UNS). UNS numbers are listed in Metals & Alloys in the Unified Numbering System, 10th ed. (Warrendale, PA: SAE International and West Conshohocken, PA: ASTM International, 2004).

INTRODUCTION

Cementite (Fe_3C) is a metastable compound[1] often classified as a 'corrosion product' although it is found in the material's microstructure. As opposed to iron carbonate ($FeCO_3$), cementite is not precipitated on the steel surface but appears as a leftover structure once the ferrite phase has partially corroded.

When considering steels with less than 0.76 wt.% C with a ferritic pearlitic microstructure, as shown on Figure 1 (a)[2,3], the microconstituents are proeutectoid ferrite and pearlite colonies, which are alternating lamellar-like layers of α-ferrite and Fe_3C. In a tempered martensitic microstructure (quenched and tempered), shown in Figure 1 (b)[2,3], there is evidence of an acicular ferrite phase with Fe_3C precipitates. Clover, *et al.*[4], have demonstrated that corrosion rate behavior of these types of steel depends on the material microstructure. It was found that a ferritic-pearlitic microstructure experiences localized corrosion, whereas a tempered martensite or ferritic microstructure undergoes uniform corrosion[4], due to preferential corrosion of the ferrite over Fe_3C.

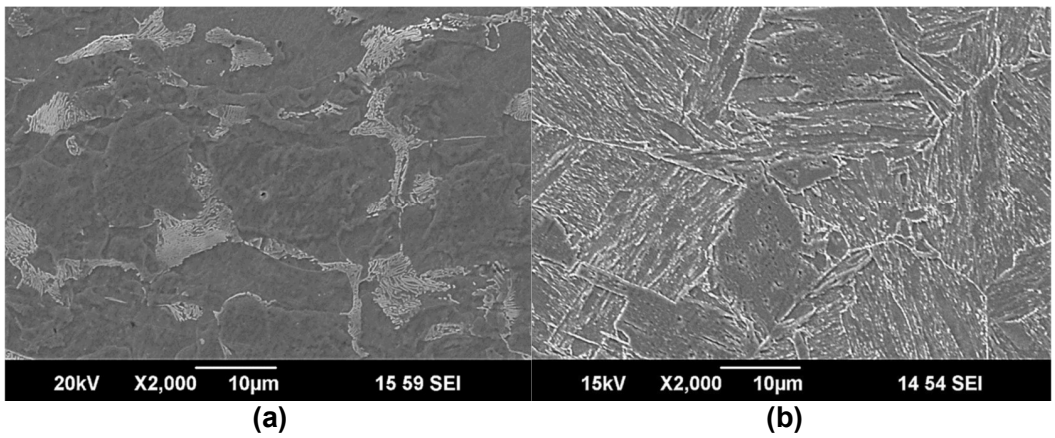

Figure 1: SEM image of (a) ferritic-pearlitic microstructure of UNS G10180 and (b) tempered martensitic microstructure of UNS G10180 after thermal treatment[2,3]

Throughout the literature, it is found that the ferrite phase behaves as an anode relative to the Fe_3C, which acts as a cathode[1-11]. Consequently, ferrite corrodes, leaving exposed Fe_3C residues on the surface of the steel[8,10,13]. The reason for this is because the electric potential of α-ferrite is -0.4 to -0.5 V and the electric potential of Fe_3C is +0.37 V[5], with respect to a standard hydrogen electrode. Additionally, the ferrite phase tends to progressively corrode at faster rates as the ratio of the cathode to anode surface area becomes larger[5], which occurs when the ferrite phase galvanically corrodes over Fe_3C, leaving a large cathode area with respect to the anode surface area.

Various researchers have studied the effect of the Fe_3C layer on the formation of $FeCO_3$. Ieamsupapong, *et al.*[12], found that the presence and nature of Fe_3C plays a governing role with regard to the formation of $FeCO_3$ on steel when using UNS G10180 ferritic-pearlitic at various pH values. His findings were similar to those of Farelas, *et al.*[13], where the authors investigated how an exposed Fe_3C layer affects $FeCO_3$ formation by testing two dissimilar carbon steels (dissimilar carbon content and microstructure). Both Ieamsupapong[12] and Farelas[13] concluded that Fe_3C acts as a diffusion barrier for ferrous ions generated through the corrosion process, increasing the surface Fe^{2+} concentration and pH and favoring the formation of $FeCO_3$ within the Fe_3C network.

Other authors came to the opposite conclusion and postulated that the exposed Fe_3C, obtained through pre-corrosion of the metal, does not have any effect on the formation of $FeCO_3$[6]. However, the authors' observations were due to the fact that most of the Fe_3C had spalled off during the experiment as

witnessed by SEM images. $FeCO_3$ still formed as the experimental conditions were set to ensure iron carbonate saturation $S(FeCO_3)$ values in the range of 300-500, which facilitated $FeCO_3$ formation even after the removal of Fe_3C.

Flow effects are said to play a major role in the formation of $FeCO_3$ within the pores of Fe_3C since it is weak and fragile[5], and thus very susceptible to removal by flowing conditions. Akeer[14,15] investigated the formation of $FeCO_3$ at high wall shear stress in a thin rectangular channel used for high velocity single phase flow experiments. Akeer performed experiments for a variety of steel types at highly turbulent conditions (τ = 535 Pa) developed from the beginning of the experiment and found that no protective $FeCO_3$ layer formed on the surface even at high bulk $S(FeCO_3)$. Additionally, the high wall shear stress also led to the removal of all iron carbide (Fe_3C) that may have formed[14].

Since high flow velocities are common in various field applications, Di Bonaventura tested various steel microstructures under flow velocities equivalent to 0.4 and 0.6 m/s in a 10" pipe with 0.3 and 0.5 Pa wall shear stress, respectively[2,3,16]. In these studies, it was found that a ferritic-pearlitic microstructure was able to retain the iron carbide layer better than other microstructures, such as tempered martensite, due to the Fe_3C distribution in the material's microstructure and the higher carbon content (0.18 wt.% C compared to 0.05 wt.% C for tempered martensitic material), which then favored $FeCO_3$ formation. Within this context, the ferritic-pearlitic microstructure was tested at higher velocities to identify if Fe_3C could be removed due to turbulence and hence impeded $FeCO_3$ formation even at favorable conditions (high $S(FeCO_3)$).

EXPERIMENTAL PROCEDURE

Experimental Setup

This set of experiments were carried out in equipment built in-house called a Thin Channel Flow Cell (TCFC), which has a thin rectangular flow channel (3 mm height, 100 mm width, 600 mm length), shown in Figure 2. This test set-up can accommodate up to 4 specimens (three for surface and cross-section characterization and one for electrochemical measurements). The pH and iron concentration of the solution were not held constant as compared to previous studies[2,13]; however, due to the large 150-liter (~40 gallon) volume of the TCFC, these parameters, which were monitored continuously, remained relatively stable throughout the course of each experiment.

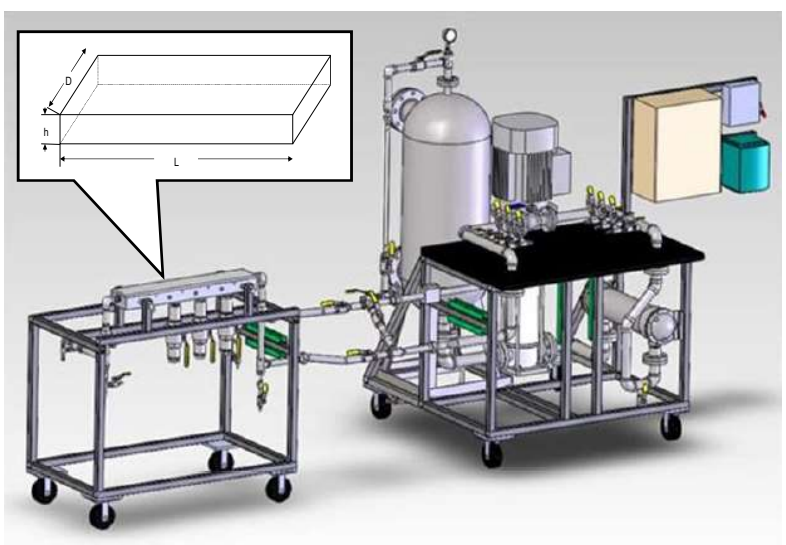

Figure 2: Thin Channel Flow Cell (TCFC) (image courtesy of Cody Shafer, ICMT)

Experiments were conducted in a 1 wt.% NaCl electrolyte with initial $S(FeCO_3)$ = 10. This saturation value ensured conditions favoring a steady $FeCO_3$ layer formation. Experiments were conducted at three different velocities (0.4, 2 and 6 m/s), enabling comparison with previous studies performed at low velocity[3,13,16], and, at the same, enabling determination a critical flow velocity for removal of Fe_3C. The equivalent pipeline velocities in a 10-inch pipe, Veq, were determined using the Sherwood correlation for a smooth pipe. Wall shear stresses, τ, were determined from correlations and direct measurements using a floating element sensor[17,18]. The duration of the experiments was five days, enabling sufficient time for Fe_3C to form, as indicated in previous experiments of this kind[2,3,12,13,16]. The other environmental conditions (pH 6.6, T = 80°C) were selected to ensure optimal corrosion product layer forming conditions, based on the literature review and analyses performed. One steel specimen was removed on the third day and two specimens were removed on the last day for surface characterization to determine the nature of the corrosion product present (if any) and for weight loss measurements. Table 1 summarizes all of the experimental parameters.

Table 1: Experimental parameters used to study the removal of Fe_3C

Experimental Setup	Thin Channel Flow Cell
Material	UNS G10180 ferritic-pearlitic
Electrolyte	1 wt.% NaCl aqueous solution
pH	6.6 ± 0.03
Temperature	80°C
Total Pressure	1 bar (10^5 Pa)
CO_2 Partial Pressure	0.53 bar (5.3 x 10^4 Pa)
Initial [Fe^{2+}]	2 ± 1 ppm
Saturation w.r.t. $FeCO_3$	10 – 30
Flow Velocity	0.4, 2 and 6 m/s
Equivalent Pipeline Velocity in 10" pipe, Veq	0.75, 4.7, and 12.0 m/s
Shear Stress, τ	0.8, 20, and 100 Pa
Surface Analysis	SEM, Raman and Cross-Section
Electrochemical Measurements	OCP and LPR

Materials

The UNS G10180 material with a ferritic-pearlitic microstructure was chosen for this set of experiments since this material had shown significant Fe_3C layer/residues of about 40 ± 20 mm thickness in previous experiments by XRD and cross-sectional analysis[2,3,16]. Table 2 provides the composition of the UNS G10180 material. The ferritic pearlitic microstructure is shown in Figure 1 a).

Table 2: Chemical composition of UNS G10180 (wt.%)

UNS G10180 (balance Fe)									
Al	**As**	**C**	**Co**	**Cr**	**Cu**	**Mn**	**Mo**	**Nb**	**Ni**
0.008	0.006	0.18	0.003	0.12	0.18	0.75	0.020	0.002	0.065
P	**S**	**Sb**	**Si**	**Sn**	**Ti**	**V**	**W**	**Zn**	**Zr**
0.011	0.021	0.009	0.16	0.009	0.002	0.003	0.014	0.004	0.003

Electrochemical Measurements

A Gamry[3] potentiostat was used for electrochemical and potential measurements. The working electrode was polarized ±5 mV versus the open circuit potential using a scan rate of 0.125 mV/s for linear polarization resistance (LPR) measurements. The B value that was used was 26 mV/decade[3,5,10,11] obtained from the literature as being typical for low temperature CO_2 corrosion of mild steel. The polarization resistance from LPR measurements was used to calculate the current density (i_{corr}, A/cm^2) and in turn the corrosion rate in millimeters per year (mm/yr) using the Stern-Geary Equation (1)[1Error! Reference source not found.,12,13] as follows:

$$\text{Corrosion rate (mm/yr)} = \frac{a i_{corr} MW}{\rho n F} \quad (1)$$

Where MW is the molecular weight of iron (g/mol), ρ is the density of iron (g/cm^3), n is the number of electrons involved in the electrochemical reaction, F is Faraday's constant, and *a* is a conversion factor to obtain corrosion rate in mm/yr units, and corrections were made of solution resistance.

RESULTS

Water Chemistry

Figure 3 and Figure 4 show changes in water chemistry, pH and ferrous ion concentration, respectively, in the TCFC set up for the UNS G10180 ferritic-pearlitic tested at three different velocities. It can be seen that some deviations from the initial pH and ferrous ion concentration are noticed, due to the fact that water chemistry could not be controlled as opposed to experiments described in previous studies[2,3,14]. Changes in water chemistry, especially in pH, can result in saturation value, S($FeCO_3$), deviations. However, changes in water chemistry were not drastic as shown in Figure 5, and did not affect the results of this set of experiments, thus, the removal of Fe_3C could be properly analyzed without any environmental factors affecting validity of the results. The saturation values shown in Figure 5 were calculated based on concentration of ferrous and carbonate ions and the solubility equation as described in other literature[2].

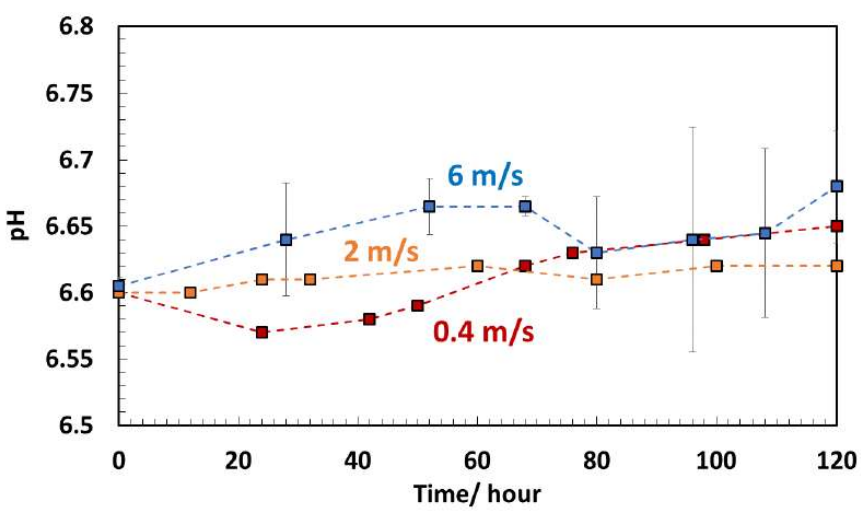

Figure 3: Comparison of pH over time for 0.4 m/s (Veq = 0.75 m/s, τ = 0.8 Pa), 2 m/s (Veq = 4.7 m/s, τ = 20 Pa) and 6 m/s (Veq = 12 m/s, τ = 100 Pa) experiments with ferritic-pearlitic UNS G10180

[3] Trade Name

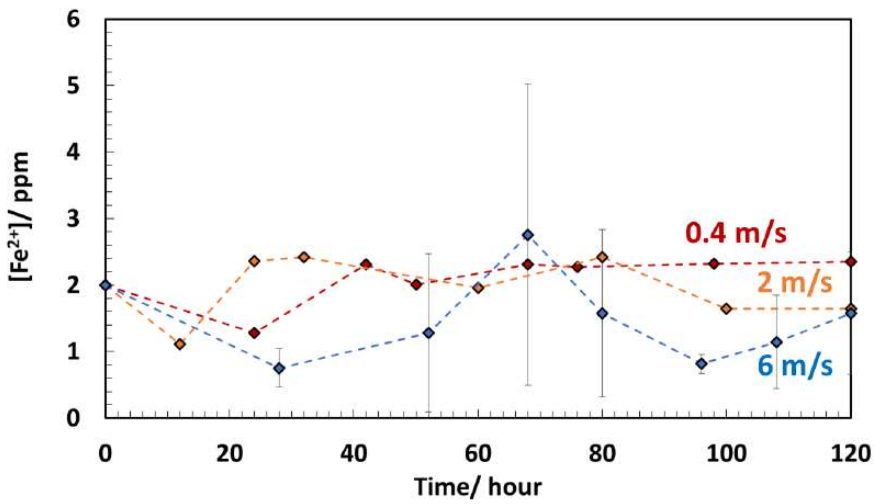

Figure 4: Comparison of [Fe^{2+}] over time for 0.4 m/s (Veq = 0.75 m/s, τ = 0.8 Pa), 2 m/s (Veq = 4.7 m/s, τ = 20 Pa) and 6 m/s (Veq = 12 m/s, τ = 100 Pa) experiments with ferritic-pearlitic UNS G10180

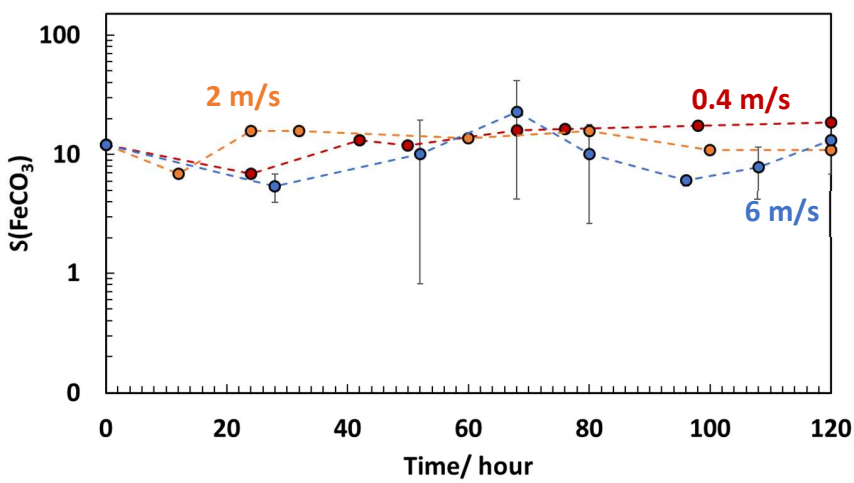

Figure 5: Comparison of S($FeCO_3$) over time for 0.4 m/s (Veq = 0.75 m/s, τ = 0.8 Pa), 2 m/s (Veq = 4.7 m/s, τ = 20 Pa) and 6 m/s (Veq = 12 m/s, τ = 100 Pa) experiments with ferritic-pearlitic UNS G10180

Corrosion Rates

Figure 6 shows LPR corrosion rate measurements during the course of the experiments with ferritic-pearlitic UNS G10180 tested at three different velocities. It can be seen that for the 0.4 m/s (Veq = 0.75 m/s, τ = 0.8 Pa) and 2 m/s (Veq = 4.7 m/s, τ = 20 Pa), the corrosion rate increased over time until it reached a value of about 7 mm/yr after about 40 hours. As seen in previous studies, this was because of the progressive exposure of Fe_3C acting as a cathodic area and causing galvanic corrosion of the anodic α-ferrite. This stage is commonly described as the active corrosion stage[2,3,12,13,16]. For the 0.4 m/s (Veq = 0.75 m/s, τ = 0.8 Pa), it can be seen that the corrosion rate starts decreasing at about the 45th hour down to a low and stable value of about 0.2 mm/yr. This can be attributed to the nucleation and growth of $FeCO_3$[2,3,12,13,16]. In comparison with results obtained from previous experiments[2,3,16], for the same conditions and velocity, there is a good reproducibility of the results, even though the experimental set ups were different.

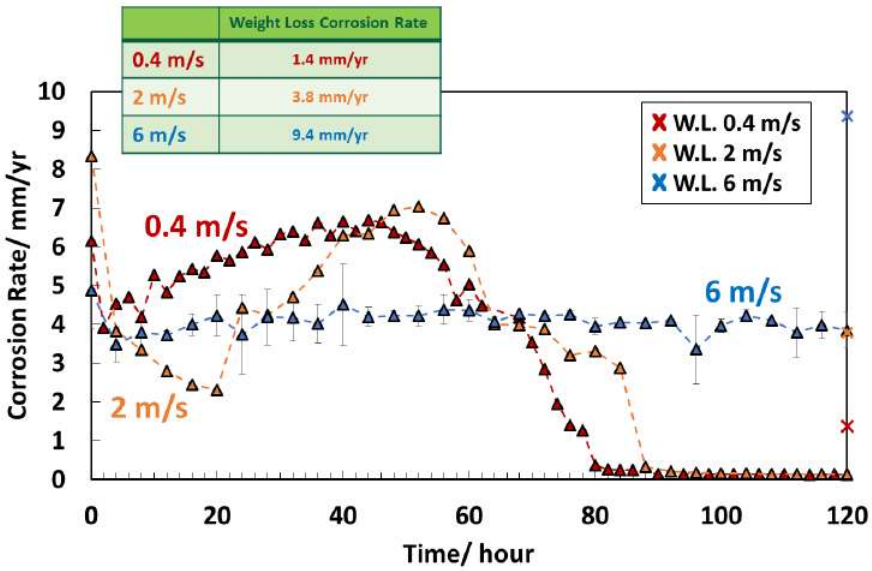

Figure 6: Comparison of LPR corrosion rate over time for 0.4 m/s (Veq = 0.75 m/s, τ = 0.8 Pa), 2 m/s (Veq = 4.7 m/s, τ = 20 Pa) and 6 m/s (Veq = 12 m/s, τ = 100 Pa) experiments with ferritic-pearlitic UNS G10180

For the 2 m/s (Veq = 4.7 m/s, τ = 20 Pa) experiments, corrosion rate started decreasing at about the 60th hour to a low and stable corrosion rate value of about 2 mm/yr, similar to the one obtained for 0.4 m/s (Veq = 0.75 m/s, τ = 0.8 Pa). The corrosion rate started to decrease at a later time than the lower velocity experiment as it took longer to reach favorable conditions (higher pH) for the formation of $FeCO_3$, due to the higher mass transfer rates. For the 6 m/s (Veq = 12 m/s, τ = 100 Pa) experiment, however, the corrosion rate was stable at a value of about 4 mm/yr, indicating absence of the active corrosion stage typically observed at lower velocities. This stable corrosion rate value is attributed to the removal of Fe_3C, which caused the corrosion rate behavior to perform similarly to that of pure iron, as seen in previous studies[2]. The high and stable corrosion rate also correlates well with Akeer's previous findings[14]. Additionally, the time averaged weight loss corrosion rate showed similar trend: for the 6 m/s (Veq = 12 m/s, τ = 100 Pa) experiment, the corrosion rate was 9.4 mm/yr, which was significantly higher than the two other measurements at lower velocities. LPR corrosion rate results shown in Figure 6 obtained from the TCFC experiments were compared with those obtained with a 4-liter, controlled mass transfer and controlled water chemistry setup described in previous studies[2,3,16]. In the previous 2-liter studies, $FeCO_3$ formed after *ca.* 100 hours at 250 rpm (Veq = 0.6 m/s, τ = 0.5 Pa). In comparison, $FeCO_3$ formation in the TCFC at 0.4 m/s (Veq = 0.75 m/s, τ = 0.8 Pa) occurred after *ca.* 40 hours.

Surface Morphologies and Characterization

Figure 7 shows the surface morphologies of the specimens taken out on days 3 and 5. For the 0.4 m/s (Veq = 0.75 m/s, τ = 0.8 Pa) and 2 m/s (Veq = 4.7 m/s, τ = 20 Pa) experiments, specimens for days 3 and 5 show similar surface morphologies with a non-uniform surface. This uneven surface confirms that the preferential dissolution of ferrite had occurred, while the Fe_3C acted as a cathode and remained on the steel surface[1,5-8,10,11,14]. The 0.4 m/s specimen surface morphology is similar to the findings from previous studies under the same environmental conditions[2,3,16], as there was some precipitation of $FeCO_3$ prisms on the surface of the specimens. The 2 m/s (Veq = 4.7 m/s, τ = 20 Pa) specimens also show some $FeCO_3$ precipitation on the steel surface. Raman spectra shown in Figure 8 and Figure 9

for 0.4 m/s (Veq = 0.75 m/s, τ = 0.8 Pa) and 2 m/s (Veq = 4.7 m/s, τ = 20 Pa) specimens, respectively, retrieved after day 5, confirm that the corrosion product was $FeCO_3$ based on spectra obtained from the literature[19-21].

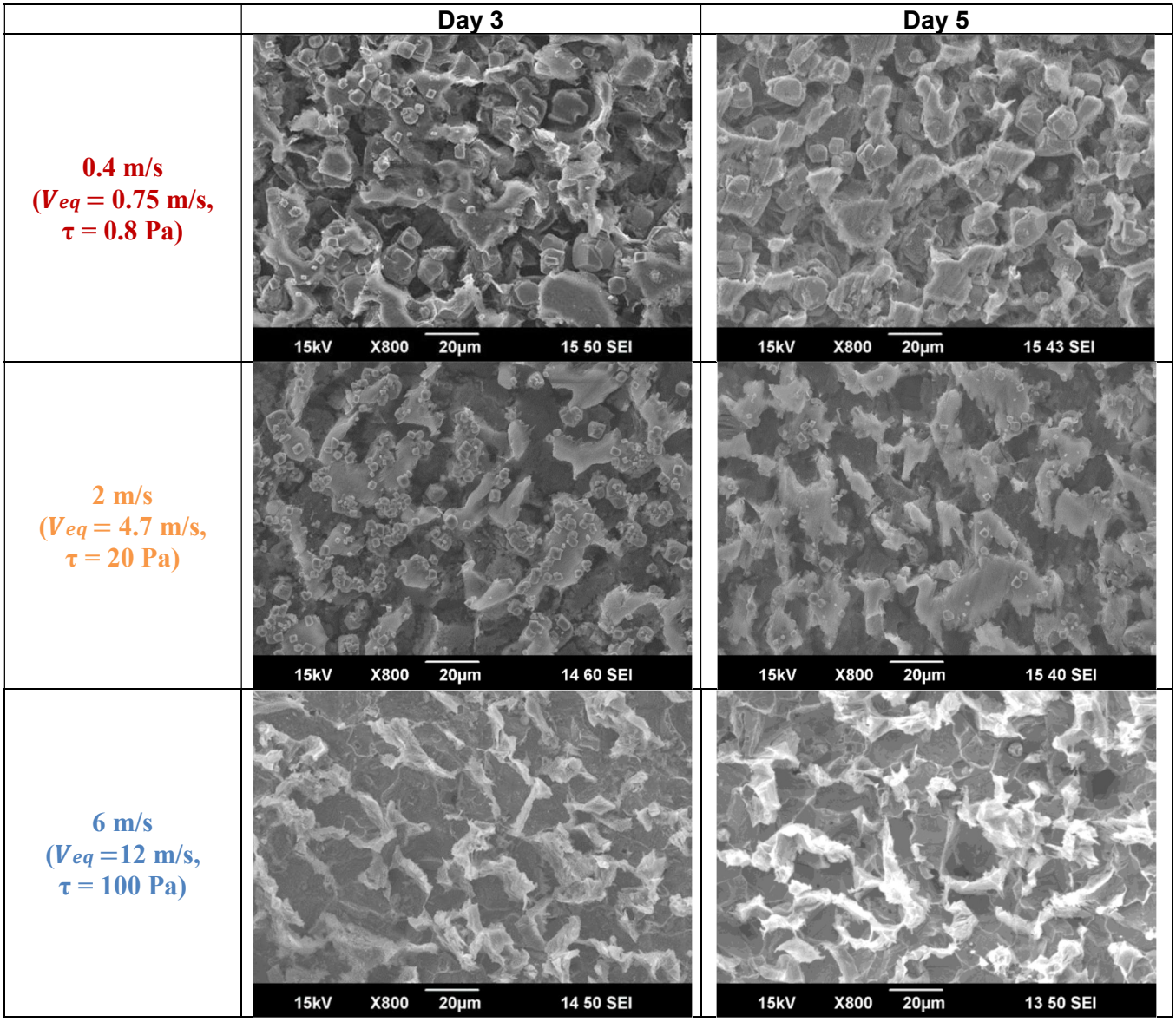

Figure 7: SEM images showing comparison of surface morphologies over time for 0.4 m/s (Veq = 0.75 m/s, τ = 0.8 Pa), 2 m/s (Veq = 4.7 m/s, τ = 20 Pa) and 6 m/s (Veq = 12 m/s, τ = 100 Pa) experiments with ferritic-pearlitic UNS G10180

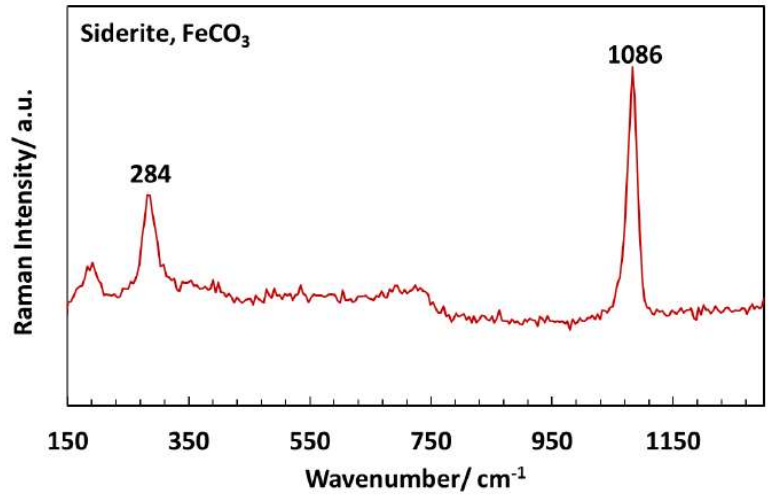

Figure 8: Raman spectra of surface confirming $FeCO_3$ as a corrosion product for 0.4 m/s (Veq = 0.75 m/s, τ = 0.8 Pa) experiment with ferritic-pearlitic UNS G10180

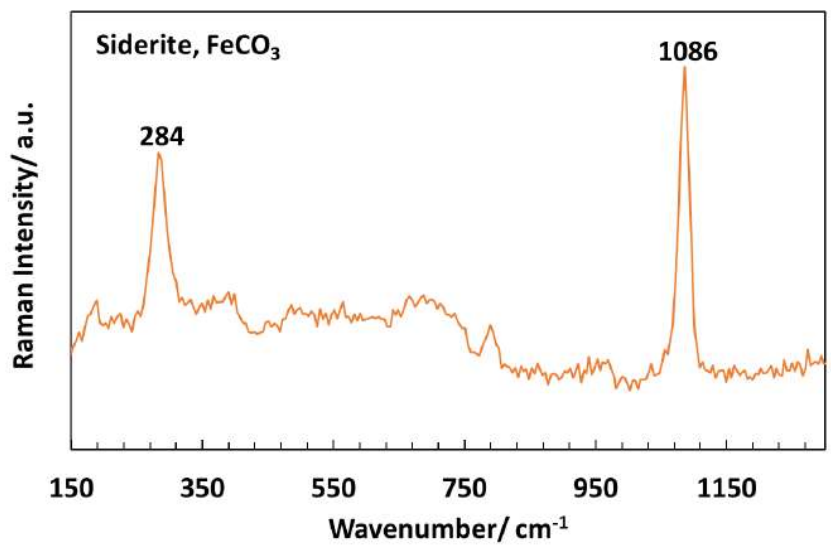

Figure 9: Raman spectra of surface confirming $FeCO_3$ as a corrosion product for 2 m/s (Veq = 4.7 m/s, τ = 20 Pa) experiment with ferritic-pearlitic UNS G10180

For the 6 m/s (Veq = 12 m/s, τ = 100 Pa) specimen, however, a bare steel surface with white residues is observed, which may be due to the removal of Fe_3C due to turbulent conditions. There was no evidence of initial polishing marks or grooves, which are indicative of carbide remaining on the steel surface[12,13]. This surface morphology shows similar results to Akeer's previous study[14]. Figure 10 (a) shows SEM images of locations used for EDS analysis in order to determine the nature of the white residues; the points labeled 1 and 2 were analyzed. Figure 10 (b) shows the EDS spectrum for the point labeled 1 which analyzes the white residue. It is noteworthy that there was enrichment of alloying elements and, as indicated by the mass% and atom% values, there was no significant presence of carbon. It is safe to assume that this was not a Fe_3C network, but rather surface enrichment with respect to the alloying elements of the UNS G10180. EDS analysis was also performed on the point labeled 2 on Figure 10 (a), which showed that this is indeed a bare steel surface as only the presence of iron was detected. This finding correlates with Akeer's previous study, where no carbide was witnessed on the surface of such a steel specimen exposed to high flow velocity[14]. For the lower

velocity experiments, the EDS results show a high carbon and oxygen content in the ranges of 10-20 atom% C, 20-30 atom% O and 60 -70 atom% Fe.

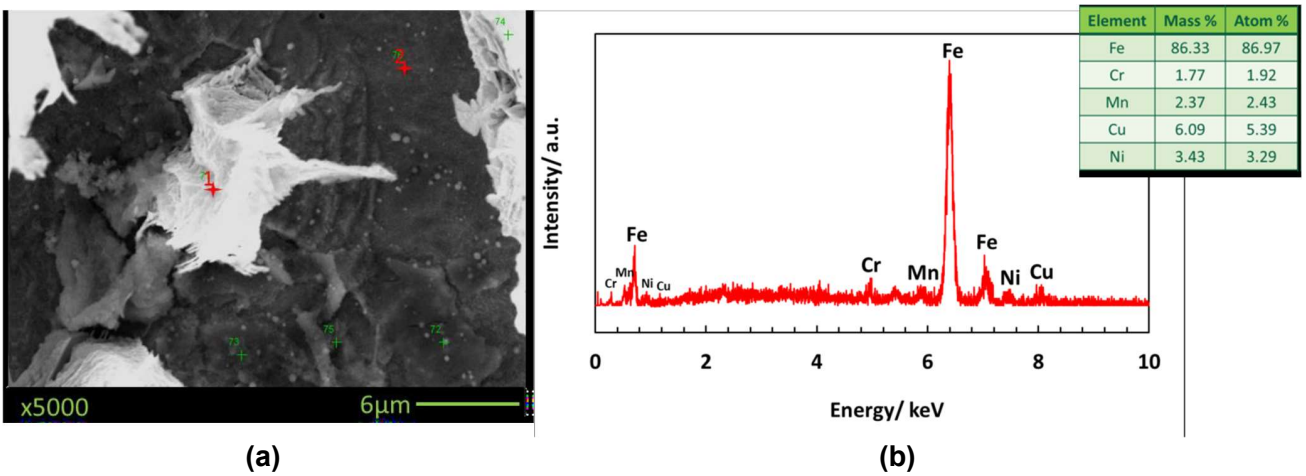

(a) (b)

Figure 10: (a) SEM image used for EDS analysis showing surface morphology after day 5 for 6 m/s (Veq = 12 m/s, τ = 100 Pa) experiment with ferritic-pearlitic UNS G10180, (b) EDS spectrum taken at point labeled 1 in (a) confirming presence of alloying elements

Raman analysis was also performed to determine if there was evidence of any corrosion product on the surface of the specimen, shown in Figure 11. It can be seen that there was no peak corresponding to siderite (1084 cm^{-1}). However, a peak was found at 693 cm^{-1}. Upon searching of the literature on Raman spectroscopy and given the content of alloying elements in the UNS G10180, shown in Table 2, it was found that this peak could correspond to $FeCr_2O_4$ (chromite)[22]. Raman spectra, surface morphologies, EDS analysis and corrosion rate trend obtained from LPR measurements confirm that no $FeCO_3$ formed on the specimen surface and no Fe_3C was retained. Fe_3C was removed by high flow velocities, similar to what Akeer established[14].

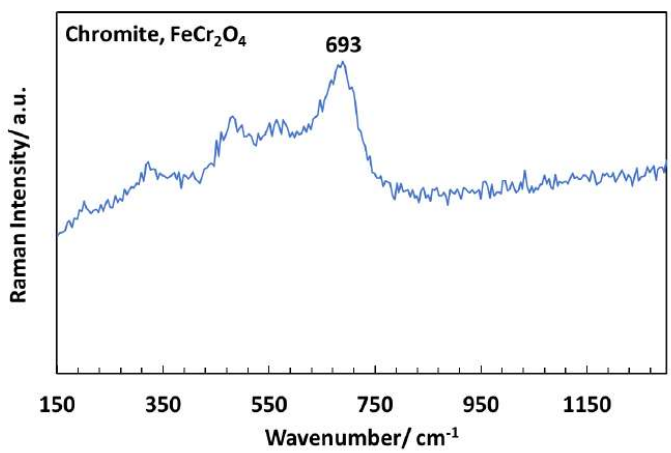

Figure 11: Raman spectra of surface for 6 m/s (Veq = 12 m/s, τ = 100 Pa) experiment with ferritic-pearlitic UNS G10180

Cross-Sectional Morphologies

Figure 12 shows cross-sectional morphologies of specimens shown in Figure 7. The 0.4 m/s (Veq = 0.75 m/s, τ = 0.8 Pa) specimens show a Fe_3C network with $FeCO_3$ precipitation, which correlates to the corrosion rate shown in Figure 6. These results are similar to what was found in the same test conditions in previous studies[2,3,16]. The 2 m/s (Veq = 4.7 m/s, τ = 20 Pa) specimen also shows a Fe_3C network with $FeCO_3$ precipitation. However, the Fe_3C network is more visible in areas where precipitation of $FeCO_3$ did not occur. On the other hand, the 6 m/s (Veq = 12 m/s, τ = 100 Pa) specimen shows no significant Fe_3C network nor $FeCO_3$ precipitation, which can further confirm that the removal of Fe_3C occurred and hence prevented the precipitation of $FeCO_3$. This can be supported by the corrosion rate trend shown in Figure 7, for the 6 m/s (Veq = 12 m/s, τ = 100 Pa) experiment, where the corrosion rate was high and stable over time[12-14].

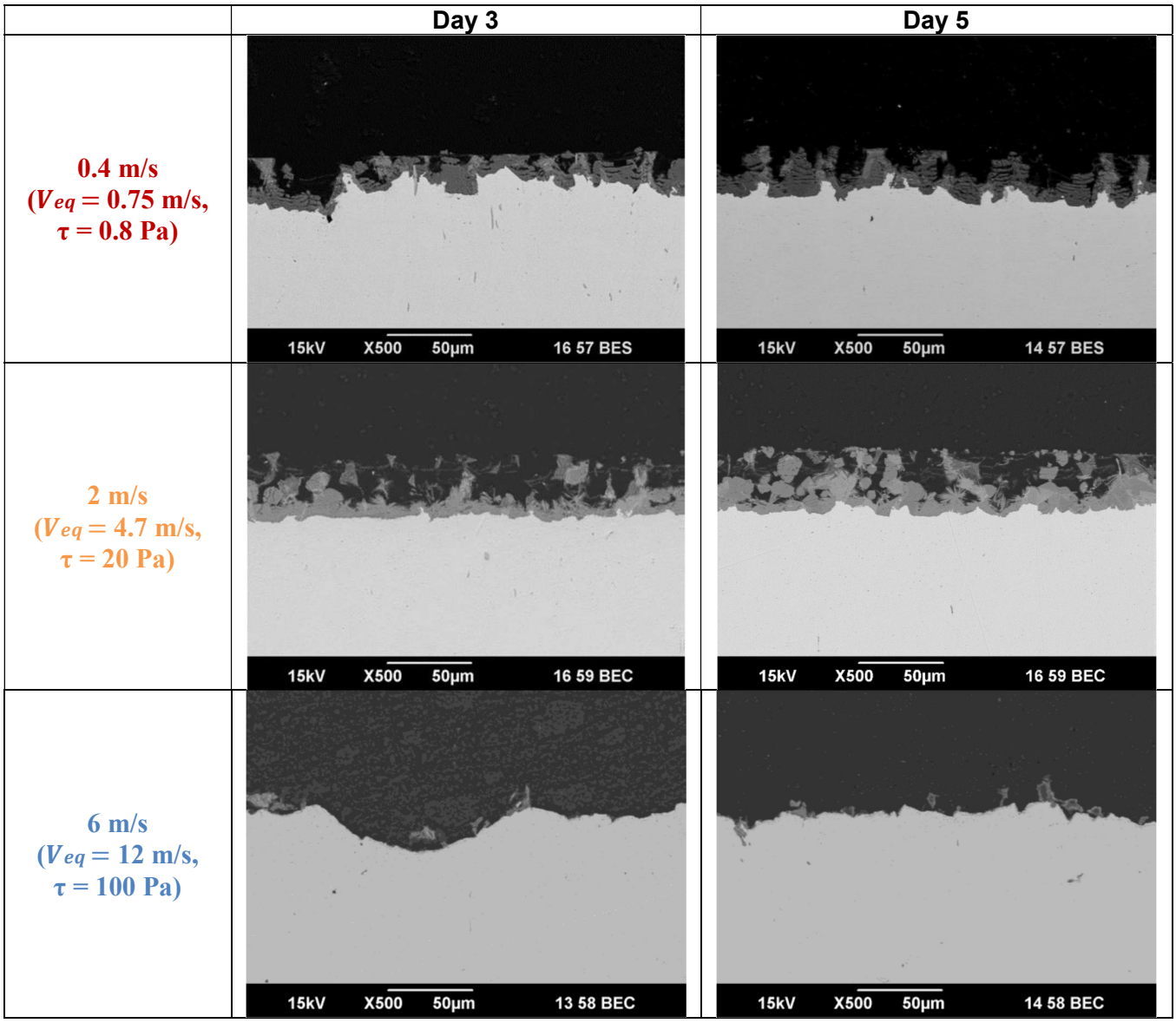

Figure 12: SEM images showing cross-sectional morphologies over time for 0.4 m/s (Veq = 0.75 m/s, τ = 0.8 Pa), 2 m/s (Veq = 4.7 m/s, τ = 20 Pa) and 6 m/s (Veq = 12 m/s, τ = 100 Pa) experiments with ferritic-pearlitic UNS G10180

CONCLUSIONS

The TCFC (A corrosion testing system with very controlled flow conditions) was used to identify the velocity required for removal of a Fe_3C layer, considering a steel with ferritic-pearlitic microstructure. At the lowest velocity tested (Veq = 0.75 m/s, τ = 0.8 Pa), similar results were obtained as in previous studies where $FeCO_3$ precipitation within Fe_3C network occurred and caused a decrease in the corrosion rate. At the highest velocity tested (Veq = 12 m/s, τ = 100 Pa), the Fe_3C layer was not retained which impeded the precipitation of $FeCO_3$ even though water chemistry was favorable at S(FeCO3) ≈ 10. These results indicate that flow can impact surface precipitation of $FeCO_3$ due to the removal of Fe_3C from the steel surface. This study provides a more relatable finding for the oil and gas industry due to the higher flow velocities tested, which are expected during operations. The study enhances the understanding on the phenomenon that high flow velocities can remove Fe_3C and hinder $FeCO_3$ nucleation.

ACKNOWLEDGEMENTS

Authors would like to thank sponsors of the Corrosion Center Joint Industry Project at the Institute for Corrosion and Multiphase Technology for their financial support (Anadarko, Baker Hughes, BP, Chevron, China National Offshore Oil Corporation, ConocoPhillips, DNV GL, ExxonMobil, M-I SWACO, Occidental Oil Company, Petroleum Institute, PTT, Saudi Aramco, Shell Global Solutions, SINOPEC, TOTAL, TransCanada, & WGK), Ali Raifei and Prof. Hugh Richardson at the Ohio University Department of Chemistry and Biochemistry for usage of analytical equipment, as well as Alexis Barxias and Cody Shafer for their assistance in the laboratory.

REFERENCES

1. W.D. Callister, D.G. Rethwisch, *Materials Science and Engineering: An Introduction*, Vol. 7. (New York, NY: Wiley, 2007), p.665-715.
2. M. Di Bonaventura, *Effect of Flow on the Formation of Iron Carbonate and Influence of Exposed Iron Carbide Layer.* (Athens OH: Ohio University)
3. M. Di Bonaventura, B. Brown, S. Nesic, M. Singer, "Effect of Flow and Steel Microstructure on the Formation of Iron Carbonate," *Corrosion* 75, 10 (2019): p. 1183-1193.
4. D. Clover, B. Kinsella, B. Pejcic, R. De Marco, "The Influence of Microstructure on the Corrosion Rate of Various Carbon Steels," *Journal of Applied Electrochemistry* 35, 2 (2005): p. 139-149.
5. A. Groysman, *Corrosion for Everybody* (Springer Science & Business Media, 2009), p. 21-29.
6. T. Berntsen, M. Seiersten, T. Hemmingsen, "Effect of FeCO3 Supersaturation and Carbide Exposure on the CO2 Corrosion Rate of Carbon Steel," *Corrosion* 69, 6 (2013): p.601-613.
7. D.N. Staicopolus, "The Role of Cementite in the Acidic Corrosion of Steel," *Journal of the Electrochemical Society* 110, 11 (1963): p.121-1124.
8. F.F. Eliyan, A. Alfantazi, "On the Theory of CO2 Corrosion Reactions – Investigating their Interrelation with the Corrosion Products and API-X100 Steel Microstructure," *Corrosion Science* 85 (2014): p.380-393.
9. S. Al-Hassan, B. Mishra, D.L. Olson, M.M. Salama, "Effect of Microstructure on Corrosion of Steels in Aqueous Solutions Containing Carbon Dioxide," *Corrosion* 54, 6 (1998): p.480-491.
10. J.L. Crolet, N. Thevenot, S. Nesic, "Role of Conductive Corrosion Products in the Protectiveness of Corrosion Layers," *Corrosion* 54, 3 (1998): p. 194-203.
11. W. Farida, T. Hemmingsen, T. Berntsen, P. Rabindran, "Effect of Precorrosion and Temperature on the Formation Rate of Iron Carbonate Film," 7th Pipeline Technology Conference, p.1-16 (2012).
12. S. Iemsupapong, B. Brown, M. Singer, S. Nesic, "Effect of Solution pH on Corrosion Product Layer Formation in a Controlled Water Chemistry System," CORROSION/2017, paper no. 9160 (Houston, TX: NACE, 2017).

13. F. Farelas, B. Brown, S. Nesic, “Iron Carbide and its Influence on the Formation of Protective Iron Carbonate in CO2 Corrosion of Mild Steel,” CORROSION/2013, paper no. 2291 (Houston, TX: NACE, 2013).
14. E. S. Akeer, *Effect of Carbon Steel Composition and Microstructure on CO2 Corrosion.* (Athens, OH: Ohio University)
15. E. Akeer, B. Brown, S. Nesic, “The Influence of Mild Steel Metallurgy on the Initiation of Localized CO2 Corrosion in Flowing Conditions,” CORROSION/2013, paper no. 2383 (Houston, TX: NACE, 2013).
16. M. Di Bonaventura, B. Brown, S. Nesic, M. Singer, “Effect of Flow and Steel Microstructure on the Formation of Iron Carbonate,” CORROSION/2018, paper no. 11179 (Houston, TX: NACE, 2018).
17. W. Li, Y. Xiong, B. Brown, K. Kee, S. Nesic, “Measurement of Wall Shear Stress in Multiphase Flow and its Effect on Protective FeCO3 Corrosion Product Layer Removal,” CORROSION/2015, paper no. 5922 (Houston, TX: NACE 2015).
18. V. C. Patel. M. R. Head, “Some Observations on Skin Friction and Velocity Profiles in Fully Developed Pipe and Channel Flows,” *Journal of Fluid Mechanics* 38, 01 (1969) p. 181-201.
19. I. Azoulay, E. Conforto, P. Refait, C. Remazeilles, “Study of Ferrous Corrosion Products on Iron Archaeological Objects by Electron Backscattered Diffraction (EBSD),” *Applied Physics A*, 110, 2 (2013): p. 379-388.
20. S. J. Oh, D. C. Cook, H. E. Townsend, “Characterization of Iron Oxides Commonly Formed as Corrosion Products on Steel,” *Hyperfine Interactions*, 112, 1-4 (1998): p.59-66.
21. C. Remazeilles, A. Dheilly, S. Sable, I. Lanneluc, D. Neff, P. Refait, “Microbiologically Induced Corrosion Process of Archaeological Iron Nails from the Sixteenth Century,” *Corrosion Engineering Science and Technology*, 45, 5 (2010): p. 388-394.
22. A. Wang, K. E. Kuebler, B. L. Jolliff, L. A. Haskin, “Raman Spectroscopy of Fe-Ti-Cr-Oxides, Case Study: Marian Meteorite EETA79001,” *American Mineralogist* 89, 5-6 (2004): p. 665-680.